Trends in Welding Research

1–5 June 1998 • Callaway Gardens Resort • Pine Mountain, Georgia

Proceedings of the 5th International Conference

Edited by
John M. Vitek
Stan A. David
John A. Johnson
Herschel B. Smartt
Tarasankar DebRoy

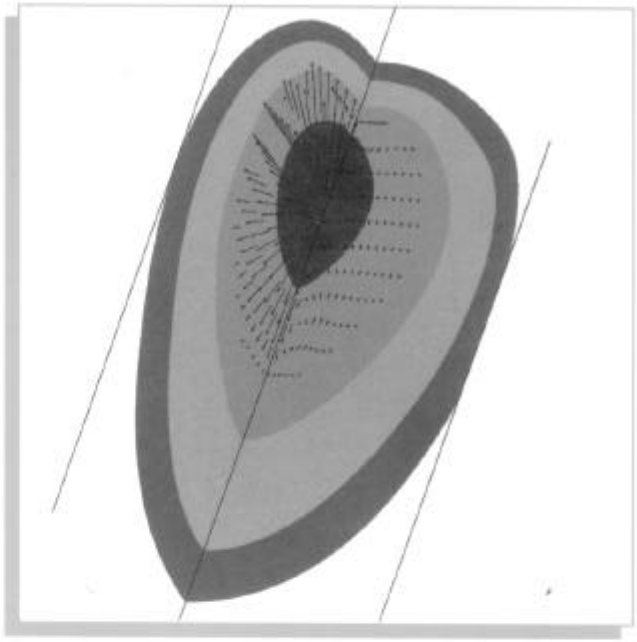

ASM INTERNATIONAL®
The Materials Information Society

AWS American Welding Society

Dissimilar Metal Welding of Copper Nickel Couple by Continuous Wave CO_2 Laser

G. Phanikumar, R. Pardeshi, K. Chattopadhyay, P. Dutta
Indian Institute of Science, Bangalore, India

J. Majumder
University of Michigan, Ann Arbor, Michigan

Introduction

Fusion weldments of dissimilar metallic joints are not well understood in the literature. Physical properties of the two metals being very different from each other lead to complexities in weld pool shape, solidification microstructure and segregation patterns[1]. If the phase diagram of the elements being joined contains intermetallic phases and possibilities of metastable phase equilibria, complexity will be increased requiring detailed analysis. Present paper reports a preliminary attempt in this direction. We have chosen Cu-Ni as the binary couple for laser joining in butt welding geometry as shown in Figure 1.

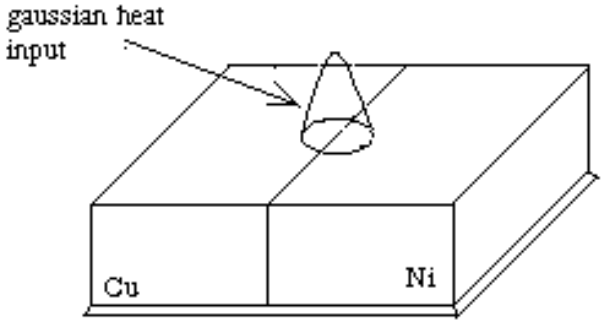

Figure 1. Schematic sketch of the dissimilar metal welding

Relevant properties[2] that play a role in the process are shown in table(1):

Table 1. Physical Properties of the binary couple.

Property	Copper	Nickel
Melting Point (^oC)	1083	1453
Thermal Conductivity ($Wm^{-1}K^{-1}$)	399	88.5
Specific Heat ($JKgK^{-1}$)	386	452
Emissivity	0.015	0.03
Density (Kgm^{-3})	8900	7905
Latent Heat (JKg^{-1})	465000	59100

As can be seen the property difference is large but the absence of any compound formation in the Cu-Ni binary system simplifies the situation for analysis.

Experiment

Commercial high purity Copper and Nickel are taken in the form of bars of square cross section of 7mm × 7mm each and are fixed on a CNC table in butt-weld geometry. Continuous Wave CO_2 laser of Trumpf make is used as the heat source. Laser diameter is 0.5mm. Scan speed is varied from $0.021ms^{-1}$ to $0.127ms^{-1}$. 30%He+50%Ar gas shroud is used to protect the liquid metal from contact with atmosphere. A limited number of experiments are also carried with pulsed Nd-YAG laser in single pulse mode with total energy varying from 200 to 345 mJ per pulse. Weld samples are cut to make transverse and longitudinal sections for characterization using Optical Micrography, Scanning Electron Microscopy, EDAX and Transmission Electron Mircoscopy.

Experimental Results: As the scan speed is decreased welding mode changes from 'conduction' to 'keyhole'. Shape of the weld pool changes from a shallow one with aspect ratio of 2 (Figure 2a) to a deep and narrow one with depth equal to the thickness of the sample as shown in Figure 2b. Shift of weld pool towards nickel is observed.

Nickel-weld interface is sharp and shows cellular growth of the base metal in to the weldment (Figure 3).

On the copper side, we notice the interface to be rough with swirls of copper-rich and nickel-rich regions in an irregular pattern (Figure 4). Copper grains are coarser near the copper weldment interface. This is not so with the nickel side. Weldment reveals cellular / dendritic microstructure.

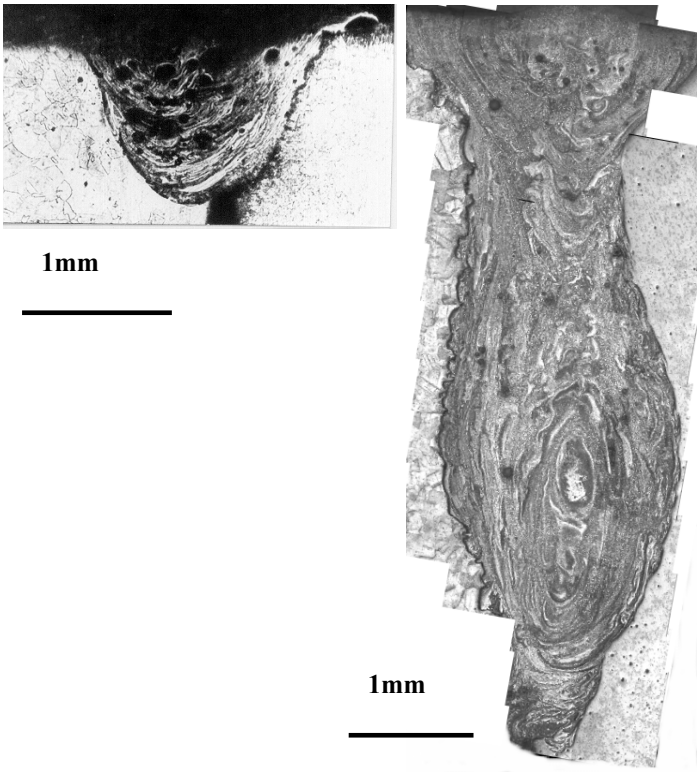

Figure2. Weld pools for scan rates a) 0.127ms^{-1} b) 0.021ms^{-1}

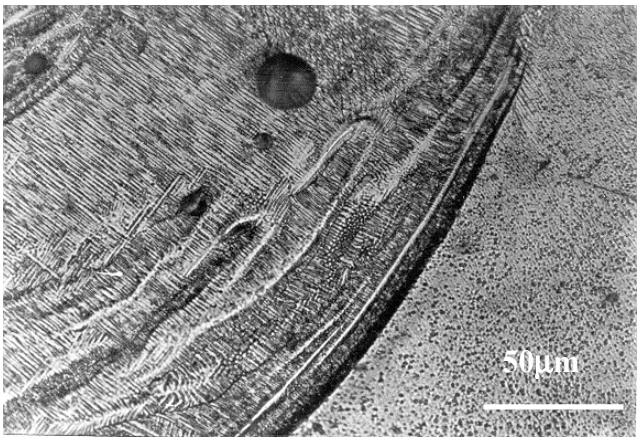

Figure3. Weldpool-Nickel Interface Microstructure

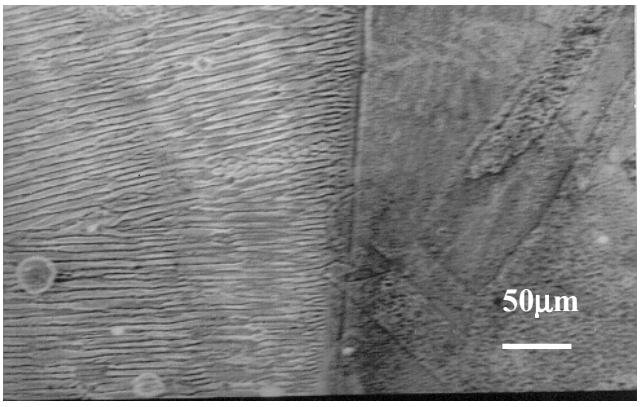

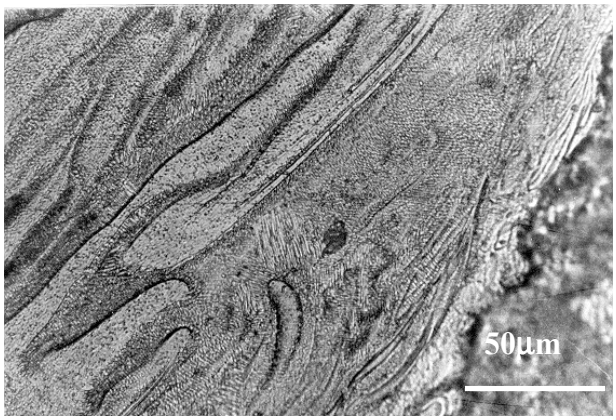

Figure 4. Weld pool - Copper Interface

Extensive banding is observed in the weldment. Etching reveals dark and bright regions depending on the composition and microstructure scale (Figure 5).

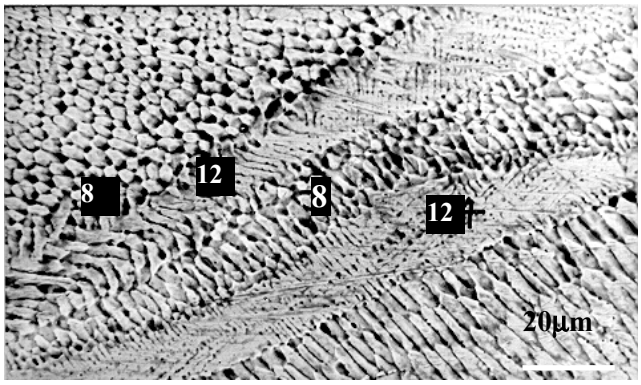

Figure5. Banding and local average copper contents (at %).

EDAX shows that the white regions are rich in copper. They also have a finer microstructural scale.

Discussion of Experimental Results: The melting of weld pool depends on the efficiency of laser coupling with Cu and Ni and their thermal properties. Nickel couples with laser more efficiently than copper and has inferior thermal transport properties. This more than compensates the higher melting point of nickel and leads to extended melting in comparision to copper. This fact is established from the shift of weld pool shape towards nickel. The solidification of melt pool is not only dictated by the freezing temperature of the local melt but also by the temporal evolution of the temperature isotherm dictated by the thermal transport. Thus it is difficult to predict which side of the weld pool starts solidifying first without a full scale modeling.

The growth from nickel side is epitaxial with a smooth interface. Initially it is planar but within few microns it shifts to columnar as dictated by the selection mode for the composition of liquid ahead of advancing interface, temperature gradients and growth rate. However this is not the same for the copper side. The swirls and the irregular patterns show that the microstructure is dominated by the pattern of

mixing. The mixing in the copper rich side is not complete and the interface does not correspond to the complete fusion zone of the copper side. This is clear from the microstructure of the top. The line marked by the arrow separates the melted region from the substrate, which is different from the mixed region that gets etched prominently.

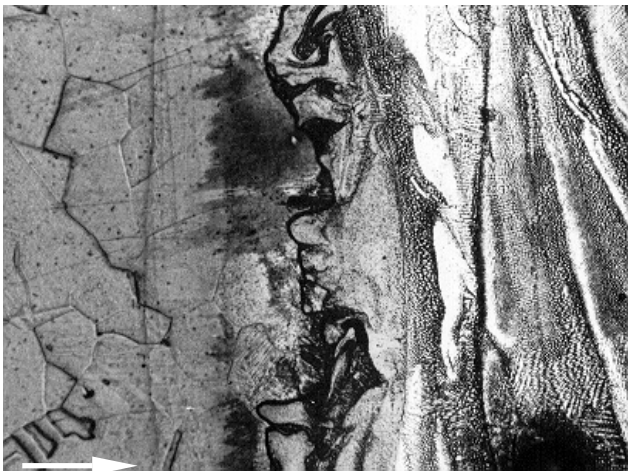

Figure6. Weldpool-Copper interface showing melted region

Microstructure of the mixed region shows cellular pattern and a combination of copper-rich and nickel-rich regions. The discontinuity in cellspacing and the compositions lead to a banded appearance. This points to a temporal change of growth conditions due to change in temperature and composition during convective mixing. Banding in the weld pool is well reported but not much discussed in literature. Our results suggest the important contribution of convective mixing for the evolution of the banded structure[7].

Computational Modeling

A full scale modelling of the dissimilar weld pool requires modeling of the melting, mixing and solidification. In the present case we attempt to model the first two processes by considering a stationary welding situation of a Cu-Ni couple. The objective is to study the asymmetry of a weld pool caused by dissimilar metal welding and associated temperature, velocity and mass fraction distributions.

In the welding of dissimilar metals, two or more metals melt and mix in the weld pool. In order to model such a phenomenon, the following two mathematical models can be used for the flow of a multi-component fluid: (1) a homogeneous mixture model, and (2) a multi-fluid model. In flow of a multi-component mixture, if we assume that the various species are mixed at the molecular level, that they share the same velocity, pressure and temperature fields etc, and that mass transfer takes place by convection and diffusion, then we can use a homogeneous model. The more complex situation where different species are mixed on larger scales, and may have separate velocity and temperature fields etc., is called 'multi-phase' flow[4, 5]. Multi-phase flow refers to the situation where more than one fluid may be present, each possessing its own flow field. In multi-phase flows, the species are mixed at much larger than the molecular length scales. They are given potentially different velocity and temperature fields etc, and these interact via empirically specified 'inter-phase transfer' terms. Simulation of such a flow would require a multi-fluid model, in which there is a separate solution field for each phase, and transport quantities interact via inter-phase transfer terms [4]. The two phases may have separate velocity and temperature fields, but there will be a tendency for these to equalize through inter-phase transfer terms.

Multi fluid models rely on constitutive relations that are difficult to determine empirically. For our simulation we are considering a homogeneous model where flow is uniformly mixed at the molecular level and is characterized by the properties assigned according to the relative proportion of each phase in the mixture. Correlations are required to provide estimates of properties in relevant flow regimes. Although some information regarding interface related quantities will be lost by assuming a homogeneous model, the present study may still give some insight into this complex problem with regard to flow field, asymmetry of pool shape, temperature field, and mixing.

Mathematical Formulation: The system used for numerical simulation is schematically shown in Figure 1. Two workpieces of copper and nickel having same dimensions are kept together. A Gaussian heat input is applied at the center such that the heat is distributed on both workpieces equally. The fluid motion is assumed to be laminar and incompressible, and the system is in unsteady state. The top surface after melting is assumed to be flat. Thermophysical properties are taken to be different for solid and liquid metals, and variation with temperature is considered. For properties of the mixtures, semi-empirical correlations are used. Surface tension, density, and viscosity are considered to be functions of temperature and mass fraction.

The conservation equations of mass, momentum, energy and mass fraction are given below:

Continuity :

$$\frac{\partial \rho}{\partial t} + div(\rho u U) = 0 \qquad (1)$$

Momentum :

$$\frac{\partial}{\partial t}(\rho u) + div(\rho u U) = -\frac{\partial p}{\partial x} + div(\mu\, grad\, u) + S_x$$

$$\frac{\partial}{\partial t}(\rho v) + div(\rho v U) = -\frac{\partial p}{\partial y} + div(\mu\, grad\, v) + S_y$$

$$\frac{\partial}{\partial t}(\rho w) + div(\rho w U) = -\frac{\partial p}{\partial z} + div(\mu\, grad\, w) + S_z \qquad (2)$$

Energy :

$$\frac{\partial}{\partial t}(\rho H) + div(\rho H\, U) = div\,(k\ \ grad\, T) + S_h \qquad (3)$$

Mass fraction :

$$\frac{\partial C}{\partial t} + div(C\, U) = div\,(D_{AB}\ \ grad\, C) \qquad (4)$$

We have used an enthalpy-porosity formulation [6] for modeling phase change and Boussinesq approximation for density variations due to heating.

Boundary Conditions : On the top surface we use a Gaussian heat flux input, and radiative and convective heat loss. The heat flux input on the top surface of the workpiece is given by,

$$q''(r) = \frac{\eta Q}{\pi\, r_q^{\,2}} \exp\left(-\frac{r^2}{r_q^{\,2}}\right) \qquad (5)$$

At the flat free surface, a balance between shear force and surface tension force is taken :

$$\mu \left.\frac{\partial u}{\partial y}\right|_{y=h} = \sigma_T \left.\frac{\partial T}{\partial x}\right|_{y=h} + \sigma_C \left.\frac{\partial C}{\partial x}\right|_{y=h} \qquad (6)$$

$$\mu \left.\frac{\partial w}{\partial y}\right|_{y=h} = \sigma_T \left.\frac{\partial T}{\partial z}\right|_{y=h} + \sigma_C \left.\frac{\partial C}{\partial z}\right|_{y=h} \qquad (7)$$

Also, at the top surface, no mass transfer is considered:

$$\frac{\partial C}{\partial y} = 0 \qquad (8)$$

At the side surfaces we consider convective heat loss, while the bottom is treated as insulated.

Discussion of Computational Results: The coupled continuity, momentum, energy, and mass fraction equations along with the boundary conditions are solved numerically using a fully implicit finite volume technique (SIMPLER algorithm [7]). The laser beam is taken as a continuous source of heat input. Transient studies are carried out till some mixing patterns are obtained. The thermophysical data for the case study is given in table 2. To avoid numerical oscillations, the iterations are underrelaxed with relaxation factor as 0.3 for the three momentum equations, 0.4 for the mass fraction equation and 0.9 for the energy equation. A non-uniform grid of 45×45×35 is used. The other parameters for the case study were taken as given in table(2).

Due to the difference in thermal diffusivity of copper and nickel, heat diffusion in copper will be more than nickel during the conduction phase of the heating process. Nickel, which has a lower thermal conductivity, will be experiencing temperature rise faster than copper. As a result, at the interface of two materials, some of the heat absorbed by nickel will be transfered to copper due to the temperature gradient. This causes a shift of the location of maximum temperature from the torch location towards nickel, which finally results in a asymmetric weld pool (Figure 7) as also observed in experiments (Figure 2).

Table 2. Process parameters used

Power of the laser :	3300 W
Radius of the beam :	1 mm
Efficiency of heat input :	60 %
Lenght of workpiece :	10 mm
Width of the workpiece :	8 mm
Height of the workpiece :	4 mm

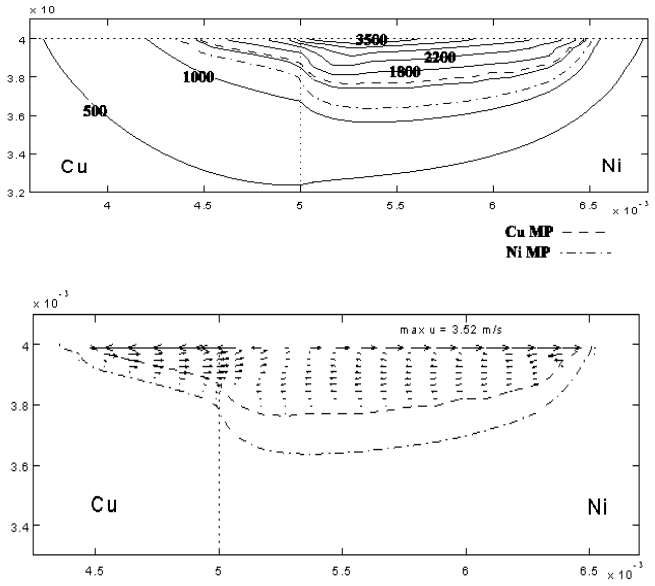

Figure7. Computed Temperature Contours and Velocity Profiles. All Temperatures are in ^{o}C

Consequently, nickel melts before copper does, even though it has a higher melting temperature than copper. After nickel starts melting, the weld pool develops a flow starting from maximum temperature and moves outwards. Since the temperature coefficient of the surface tension σ_T is negative, the value of the surface tension at the maximum temperature location is lower than that at the edges of the weld pool. Hence, the fluid in the center is pulled radially outward. From the figure, it can be seen that due to convection, isotherms bend and become non-circular. On the free surface, convection brings the hot liquid from the maximum temperature location to the edges of the weld pool, which increases the width of the weld pool. This flow also brings the cold fluid from the bottom of the pool to the surface. The amount of heat transported in the vertical direction is therefore relatively small. Hence, the melt pool tends to be shallow and wide. Since surface tension forces are dominant, the maximum velocity occurs on the free surface. Therefore, the eye of the convection cell is close to the surface.

Comparison with Experimental Results: Our computational studies have been performed for the case of stationary spot welding. An asymmetric shift of the Cu-Ni weld pool is shown in figure 8a. For comparison, spot welding experiments have been performed for the Cu-Ni couple with

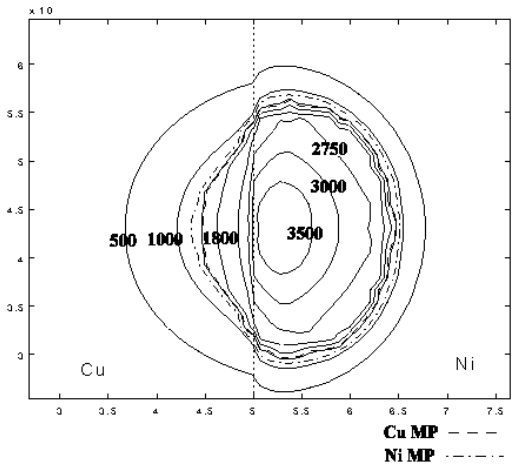

an Nd-YAG laser as shown in figure 8b, and the qualitative agreement of the weld pool shift is found to be good.

Figure 8a.Calculated Temperature contours of top surface.

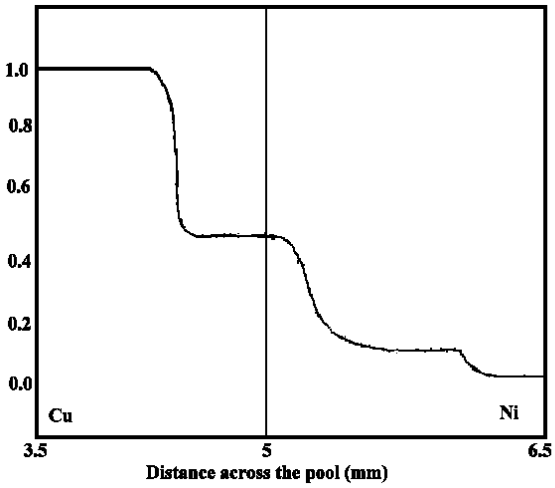

Figure 9a. Calculated Copper mass fraction Profile across a transverse section near the surface.

Variation of mass fraction of copper across the weld pool has been computed and plotted as shown in figure 9a. This agrees very well with the corresponding experimental results shown in figure 9b.

Conclusions

Laser welding of dissimilar materials consisting of a copper-nickel couple has been studied both experimentally and numerically. The experimental observations reveal several complex features of dissimilar metal welding. A preliminary attempt has been made to computationally model this complex phenomenon. In spite of some simplifying assumptions, the model is able to capture some of the key features of the process observed experimentally. This work lays a strong foundation for future studies of some of the complex issues in dissimilar joints.

Figure 8b. Top view of a spot weld taken with Nd-YAG laser with a 300 mJ pulse.

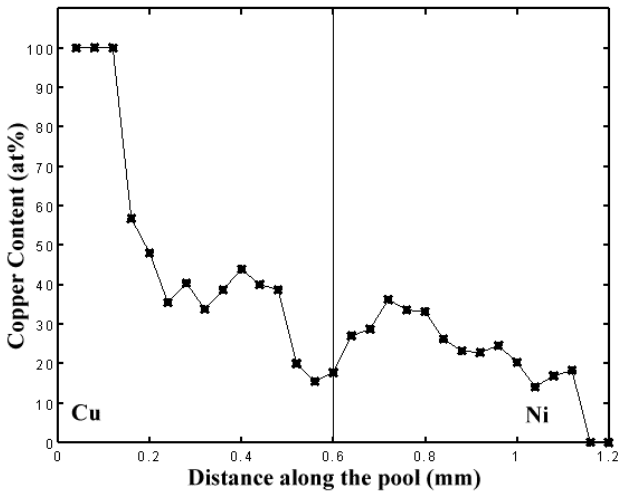

Figure 9b. Experimental Composition profiles of transverse section near the top.

References

1. Sun, Z., and Ion, J.C., *Journal of Materials Science*, 30, pp.4205-4214, (1995).

2. Eric A. Brandes, *Smithells Metals Reference Book*, Sixth Edition, Butterworths & Co Publications Ltd., 1983, London.

3. S. V. Patankar, *Numerical Heat transfer and fluid Flow*, Second Edition, Hemisphere Publications, New York (1980).

4. Caver, M. B., *Journal of Fluid Engg*., 106, pp. 147-153, (1984).

5. Ishii, M., and Mishima, K., *Nuclear Engg. and Design*., 82, pp 107-126, (1984).

6. Brent, A. D., Voller, V. R., and Reid, K. J., *Numerical Heat Transfer*, 13, pp 297-318, (1988).

7. P. A. Carvalho, A. M. Deus, R. Colaco and R. Vilar , *Acta Materialia*, 46, 5, pp 1781-1792 (1998).

Acknowledgements

The work derived support from Office of Naval Research, USA, under the Indo-US program or research co-operation (Grant No. N00014-95-1-0073).

Nomenclature

q"(r)	Heat Flux at top
η	efficiency
Q	Laser Power
r_q	Laser Beam Radius
μ	Viscosity
u,v,w	Velocities along x,y,z
T	Temperature
σ_T	Thermal Surface Tension Coeff.
σ_C	Solutal Surface Tension Coeff.
C	Solutal Weight Fraction
ρ	Density
T	Time
U	Scan Velocity
p	Pressure
S_h,S_u,S_v,S_w	Source Terms
H	Enthalpy
k	Thermal Conductivity
D_{AE}	Solutal Difusivity